Rodrigo Bort, M.; Martínez Climent, A.; Liberos Mascarell, A.; Fernández-Avilés, F.; Berenfeld, O.; Atienza, F.; Guillem Sánchez, MS. (2017). Technical Considerations on Phase Mapping for Identification of Atrial Reentrant Activity in Direct- and Inverse-Computed Electrograms. Circulation Arrhythmia and Electrophysiology. 10(9):1-13. https://doi.org/10.1161/CIRCEP.117.005008

Technical considerations on phase mapping for identification of atrial reentrant activity in direct and inverse-computed electrograms

Rodrigo - Phase Mapping of Atrial Reentrant Activity

Miguel Rodrigo, PhD[1], Andreu M. Climent, PhD[2], Alejandro Liberos, PhD[2], Francisco Fernández-Avilés, MD, PhD[2,3], Omer Berenfeld, PhD[4], Felipe Atienza,* MD, PhD[2,3], Maria S. Guillem,* PhD[1]

[1] ITACA Institute, Universitat Politècnica de València, Valencia, Spain. Camí de Vera s/n 46022.
[2] CIBERCV, Hospital General Universitario Gregorio Marañón, Instituto de investigación sanitaria Gregorio Marañón, Madrid, Spain.
[3] Facultad de Medicina. Universidad Complutense de Madrid, Madrid, Spain.
[4] Center for Arrhythmia Research, University of Michigan, Ann Arbor, USA. 2800 Plymouth Road 48109 MI.

*Dr. Atienza and Dr. Guillem share senior authorship

Address for correspondence:

Maria S. Guillem: ITACA, 1ªplanta, Edificio 8G, Ciudad Politécnica de la Innovación, Universidad Politécnica de Valencia, Camino de Vera sn 46022 Valencia (Spain), Tel. +34 96 387 79 68, Fax +34 96 387 72 79, email: mguisan@eln.upv.es

Word count: 6396/7000

Journal Subject Terms: Atrial Fibrillation, Electrophysiology

ABSTRACT

Background: Phase mapping has become a broadly used technique to identify atrial reentrant circuits for ablative therapy guidance. This work studies the phase mapping process and how the signal nature and its filtering affect the reentrant pattern characterization in EGM, Body Surface Potential Mapping (BSPM) and Electrocardiographic Imaging (ECGI) signals.

Methods and Results: EGM, BSPM and ECGI phase maps were obtained from 17 simulations of atrial fibrillation (AF), atrial flutter (AFL) and focal atrial tachycardia (AT). Reentrant activity was identified by singularity point recognition in raw signals and in signals after narrow band-pass filtering at the Highest Dominant Frequency (HDF). Reentrant activity was dominantly present in the EGM recordings only for AF and some AFL propagations patterns, and HDF filtering allowed increasing the reentrant activity detection from 60% to 70% of time in AF in unipolar recordings and from 0% to 62% in bipolar. In BSPM maps, HDF filtering increased from 10% to 90% the sensitivity, although provoked a residual false reentrant activity ~30% of time. In ECGI, HDF filtering allowed to increase up to 100% the time with detected rotors, although provoked the apparition of false rotors during 100% of time. Nevertheless, raw ECGI phase maps presented reentrant activity just in AF recordings accounting for ~80% of time.

Conclusions: Rotor identification is accurate and sensitive and does not require additional signal processing in measured or noninvasively computed unipolar EGMs. Bipolar EGMs and BSPM do require HDF filtering in order to detect rotors at the expense of a decreased specificity.

Key terms: reentrant activity; atrial rotors; electrocardiographic imaging; body surface potential mapping; electrogram; phase mapping.

INTRODUCTION

Reentrant propagation of electrical activity plays a decisive role in the perpetuation of atrial tachy-arrhythmias. While atrial flutter (AFL) is caused by a macroreentrant circuit around anatomical and/or functional obstacles that can be terminated ablating the critical isthmus[1], the nature of the waves' mechanisms that maintain atrial fibrillation (AF) is still controversial[2]. Fibrillatory electrograms analyzed using rules developed for organized rhythms, such as activation mapping[2], are unreliable due to inconsistencies in the estimated activation times in relation to the presence of far-field intra-chamber crosstalk, noise or multicomponent EGMs[3]. On the other hand, the value of sequential mapping during AF is limited due to the dynamic changes in activation sequence during AF. Despite these limitations, there is substantial experimental and clinical evidence, based on activation phase and frequency analyses, demonstrating that AF is maintained by functional reentries, or rotors, and that localized ablation of the atrial regions harboring such rotors can terminate AF episodes[4-5].

Recent progress in ablative therapies for AF has been paired with increased understanding of the wave mechanisms responsible for AF as a direct consequence of the development of novel mapping systems to characterize spatiotemporal patterns of AF electrical activity. These mapping systems include experimental optical systems based on the use of potentiometric dyes[6], or clinical electrical recording systems using multipolar catheters[5]. Phase analysis of optical mapping signals has become the most reliable method to identify reentrant patterns, since pivoting activity naturally renders singularity points (SPs) in the phase maps that can be clearly identified[7]. However, optical mapping dyes are toxic in the clinical setting and the extrapolation from experimental optical mapping to clinical electrode-based

mapping lacks validation and raises the possibility of false association of phase SPs with AF reentries, since non-reentrant electrical activity may also cause the appearance of SPs under certain circumstances. On the other hand, multi-electrode mapping catheters have difficulties to consistently map global biatrial activation with uniform accuracy. Moreover, activation time mapping that has been used to map AF[5], can be ambiguous because of multicomponent EGMs and result in inconsistencies in the estimated activation times and wave descriptions[2]. To overcome the ambiguity in marking the activation time, the phase analysis is considering the whole cardiac activation cycle indiscriminately[6]. However phase mapping techniques, as other techniques as well, make use of temporal signal filtering for improving the interpretation of propagation and reentrant pattern identification[8-9], adding another possible uncertainty into wave propagation studies in AF.

More recently, noninvasive systems have emerged as a panoramic mapping approach for simultaneous body surface recordings of biatrial activation during AF. Body Surface Potential Mapping (BSPM)[8,10], uses tens of electrodes for the analysis of surface ECG signals, while the electrocardiographic imaging (ECGI)[11] computationally reconstructs the epicardial electrical activity from the BSPM recordings. However, the accuracy of those technologies on determination of the driving role of observed rotors in human AF has not been established. Therefore, in this study we utilize mathematical models of different atrial reentrant arrhythmias to provide a robust characterization of invasive and non-invasive mapping approach for localization of reentrant activation patterns in AF. The objective of the present study is to analyze the phase mapping processes in EGM, BSPM and ECGI, including the effects of signals nature, temporal filtering and an automatic detection of SPs in

phase maps, to outline the validity and potential clinical use of those AF mapping approaches.

MATERIALS AND METHODS

Atrial mathematical models

A realistic 3D model of the atrial anatomy composed by 284,578 nodes and 1,353,783 tetrahedrons (673.4±130.3 μm between nodes) was used to simulate the atrial electrical activity[12]. A gradient on the electrophysiological properties of the atrial myocardium, specifically on $I_{k,ACH}$, I_{K1}, I_{Na} and I_{CaL}, was introduced into the atrial cell formulation[13] to obtain propagation patterns maintained by rotors. Fibrotic tissue was modeled by disconnecting a percentage of nodes between 20% and 60%, and scar tissue by disconnecting 100% of nodes in the scar region. The system of differential equations was solved by using Runge-Kutta integration based on a graphic processors unit (NVIDIA Tesla C2075 6G)[14].

An ensemble of 17 different arrhythmic electrical patterns was simulated, divided into 4 groups according to the nature of their activation patterns. Group I was composed by one AF pattern driven by multiple rotational sources and 4 AF patterns driven by a single rotor at varying locations of the LA: Pulmonary Veins (PV), Posterior Wall of the Left Atrium (PLAW) and Right Atrial Appendage (RAA). Group II was composed by 4 AFL patterns: a typical AFL, a clockwise atypical AFL, an Inferior Vena Cava (IVC) atypical AFL and an atypical AFL turning around the Pulmonary Veins (PV) due to the existence of inactive scar tissue in the PLAW. Group III was composed by 4 focal Atrial Tachycardia (AT) models repeatedly stimulated at different locations of the atria (IVC, LSPV, RIPV and RAA). Group IV was composed by the same AT simulations of Group III in which scar regions were added in order to create more

complex propagation patterns.

Electrical signals generation

For each simulation, a uniform mesh of 2048 unipolar EGMs was calculated surrounding the epicardial surface (1 mm distance) under the assumption of a homogenous, unbounded and quasi-static conducting medium by summing up all effective dipole contributions over the entire model[15]. Computed electrograms were stored for processing at a sampling frequency of 500 Hz. Bipolar electrograms were obtained as the potential difference between each node and the nearest neighbor.

The BSPM potentials on the torso model were calculated by solving the Forward Problem with the Boundary Element Method[16] in a mesh formed by 771 nodes and 1538 triangular patches (**Figure** 1). White Gaussian noise was added to the BSPM signals with a signal-to-noise ratio of 60 dB and all signals were then referenced to the Wilson Central Terminal.

Inverse-computed EGMs (ECGI signals) were obtained by solving the inverse problem with zero-order Tikhonov's regularization method and election of the regularization parameter based on the L-curve[16-17].

To evaluate the performance of an automatic rotor identification technique, epicardial EGMs of atrial scenarios with real reentrant activity were randomly re-assigned to different nodes[18]. This random epicardial EGM maps were processed as described above to obtain the BSPM and then the corresponding ECGI signals for the rotor analysis.

Signal filtering

Baseline EGM, BSPM and ECGI signals were estimated by decimation to 12.5 Hz

and filtering with a Butterworth 10th-order low-pass filter with a cut-off frequency of 2 Hz. Signals were interpolated to 500 Hz and subtracted from the original signals. EGM, BSPM and ECGI signals were then low-pass filtered with a 10th-order Butterworth filter with a cut-off frequency of 30 Hz. Processing procedures here were similar to clinical procedures elsewhere[10].

For DF analysis, EGM, BSPM and ECGI signals were baseline-removed as previously reported[10] and were then low-pass filtered with a 10th-order Butterworth filter with a cut-off frequency of 10 Hz. Power spectral density of all signals was computed using Welch periodogram (65536 point FFT and 80% overlap) to determine the local Dominant Frequency (DF) with a spectral resolution of 0.01Hz[10].

We also tested the effect of narrow band-pass filtering of EGM, BSPM and ECGI centered at the Highest DF (HDF) found on the atrial surface by using a cascade of high-pass elliptic filters with a cut-off frequency equal to HDF - 1 Hz and a low-pass elliptic filter with a cut-off frequency equal to HDF + 1 Hz[8].

Reentrant activity identification

Reentrant wave localization was carried out by identification of singularity points (SP) in the phase signal map obtained with the Hilbert Transform[19]. As shown in **Figure** 2, the phase transformation assigns a phase value between –π and π for each sample of the signal, and thus each phase corresponds to a given state of the action potential (π for resting, π/2 for depolarization, 0 for plateau and –π for repolarization). A phase map snapshot, therefore, allows inferring the propagation patterns and specifically the center of a pivoting rotor appears as a point in which phase is not defined (hence the term singularity point; SP) surrounded by phases ranging monotonically from –π to π.

In order to identify SPs, phase values were evaluated along 3 different circles surrounding each tested point with increasing radii. Six to twelve points per circle were used for the phase analysis in which the EGM, BSPM and ECGI signals were interpolated by a weighted average of the neighboring nodes, being d^{-2} the weight for each node and d the distance between nodes.

A tested point was assigned to be an SP only when the phases of at least two of these three circles was gradually increasing or decreasing for a total of 2π[8], and if the mean phase error with respect to a straight line was lower than a threshold: 0.4 radians for EGM, 0.2 radians for BSPM and no threshold for ECGI.

Testing with circles of various radii (**Figure** S1), radii of 0.5, 1 and 1.5 cm were found to maximize sensitivity of SP identification in AF models, for both raw and HDF filtered signals, and therefore selected for the study.

An SP reflects the instantaneous condition of phase reentry. Thus, a pivoting excitation pattern was considered to constitute a propagating wave when maintaining a sequential connection between its SPs across time. The distance between SPs at consecutive time instants should be less than 1 cm (EGM and ECGI) or 5 cm (BSPM) to be considered related and maintain a continuity of the wave rotation. In **Figure** S2 we show the effect of this spatial threshold on true/spurious rotor identification. Finally, only long lasting SP describing waves that complete at least two rotations were considered as rotors and other SPs were discarded.

Sensitivity and specificity calculation

The different filtering strategies were evaluated in their ability to identify stable reentrant patterns (>2 rotations) in our models of AF as functional reentries (rotors) and in AFL patterns as anatomical reentries. Different criteria for considering a

detected SP as true or false were applied for the atrial EGM and ECGI maps versus the BSPM. In EGM and ECGI maps, the sensitivity and specificity measures were based on SP location criterion, due to the implication in the ablation guidance of the SP location while in the BSPM the location of the detected SP have no direct implication and therefore sensitivity and specificity measures considered only a presence or absence criterion.

Accordingly, when the EGM and ECGI maps were analyzed on the atrial wall, excluding valves and veins, only AF rotors detected less than 1.5 cm from the actual rotor core were considered as true-location positives (named as true rotors in **Figures** 4, 5 and 7), whereas AF rotors detected >1.5 cm from the actual rotor core were considered as false-location positives. We chose 1.5 cm as a threshold distance based on the rotor precession distance in our database, which was below this value (see **Figure** S3).

In our AFL simulations a reentry was present around the TV, LPVs or IVC and its counter rotating wave was in the IVC or PV orifices, or at the septum. Therefore, in our AFL simulations the electric re-entrant pattern should generate phase singularities only inside the orifices or the septal areas. As the EGM and ECGI time-series signals in the sensitivity and specificity analysis were not calculated at the orifices and the septal areas, all SPs detected during AFL are necessarily considered as false-location positives.

When the electrical activity was analyzed on the torso surface (BSPM) the sensitivity and specificity measures were based on an SP presence criterion. In this case, the re-entrant electrical patterns generated by AF and AFL simulations can generate a rotor anywhere accross the surface[8], so only their presence or absence were considered and not their location as in EGM or ECGI maps. Therefore, all surface

reentries detected during AF and AFL patterns were considered as true-presence positives.

Additionally, reference sensitivity and specificity analyses of SP detections were as follows: (i) all SP detections (>2 rotations) during random distributions of the EGMs were considered as false positives, and (ii) all SP detections during AT and AT+scar rhythms which were simulated to be maintained by periodic focal stimulation were considered false positives.

Statistical analysis

All measures of continuous variables are reported as average ± standard deviation, and displayed as bars with a height equal to the average and whiskers length equal to the standard deviation. Statistical significance of differences between normally distributed continuous variables was estimated using the student's t-test. Linear fitting for phase measurements was carried out by using the least squares method; R-square were calculated as the coefficient of determination and phase errors were calculated as the square difference between phase measurements and their linear best-fitting. A $p<0.05$ was considered to be significant.

RESULTS

Restrictions in rotor identification

We found that we were able to identify more SPs in random EGM activity than in rotor-driven AF models (**Figure** 3.D), and phase transitions around SPs that arise from non-rotating activity were less gradual than those arising from rotational activity. In **Figure** 3.A-B the phase transitions in three concentrical circles around detected SPs are shown for a rotational and a wave break pattern from an AF simulation. In

this example, deviation from a linearly gradual change transition was largest in the outermost circle (1.5 cm radius) for the wave break pattern since phase was not monotonically increasing. Overall, this deviation was larger in the random patterns than in rotor-driven AF (1.00±0.04 vs 0.47±0.20 rad, $p<0.01$). In order to reject spurious SP detections a linearity threshold (0.4 rad) was applied to SP detections, resulting in a reduction in the amount of detected SPs, as it can be observed in **Figure** 3.D.

Transient SPs can also be found in our phase maps that arise from U turns around scars from an AT+scar simulation instead of from actual functional rotations. In **Figure** 4 one of such examples is depicted. Overall, if a duration of 0.5 turns is required to SPs to be considered as rotors, all false detections in random propagation patterns are rejected (**Figure** 4.D), while most true rotation patterns are detected (66.5±47.2% of time for AF models). However several false positives are detected (6.5±14.1% of time for AF patterns, 32.9±24.5% for AFL patterns or 57.9±43.6% for AT+scars). Since SPs that do not arise from an actual rotation transiently disappear from the phase maps without completing a rotating cycle (**Figure** 4.C), imposing a duration threshold of 2 turns reduces considerably the amount of false detections (to 0% for AF, 0% for AFL and 15.9±28.8% for AT+scar) while keeping almost unaltered the detection of true rotors (60.0±54.7%). **Figure** S4 from Supplemental Material shows rotor detection sensitivity when considering 0.25 to 4 rotations, were the incidence of spurious rotors detected in patterns other than AF decreases with the number of required rotations.

The reported detection ratio for AF models can be increased by preprocessing the EGMs before performing the phase transformation. Hilbert's transform is particularly well suited for smooth or sinusoidal signals and therefore, a band-pass filter, centred

at the activation rate allows increasing the detection ratio (from 60.0±54.7% to 70.9±39.9%) for AF models while the false positive rate detection in AF models is only 2.6±5.1% (**Figure** 5). This band-pass filtering was required for detecting rotors by using EGMs with multiple deflections, as found in bipolar EGMs. In bipolar EGMs, rotors were detected with the same detection rate than in unipolar EGMs but only after band-pass filtering (**Figure** 5.C-D and **Figure** 5.F).

However, the increased sensitivity for AF rotors detection after band-pass filtering takes place at the expense of increasing the detection ratio in AFL models, with up to 47.9±55.3% of time with detected rotors. **Figure** S5 shows an example of a stable macro-reentry around the inferior vena cava. Here, the upward propagation in the RA is followed by propagation through the Bachman's Bundle and subsequent downward depolarization of the posterior wall of the LA. This pattern was not reflected into a stable SP in the EGMs, but got smoothened and stabilized after HDF filtering and a SP appeared. Therefore, HDF filtering may increase the false positive detections that arise from actual rotating patterns -but not rotors- in the tail of the propagating wavefront.

Reentrant activity in BSPM and ECGI

We have previously proposed to apply HDF filtering to BSPM during AF in order to increase the sensitivity of rotor detection[8] but were unable to quantify the specificity of the method and whether it could be applied for computation of the ECGI maps. As shown in surface BSPMs for different mathematical models with and without HDF filtering (**Figure** 6), stable rotors can be observed after HDF filtering but not on the raw signals. However, HDF filtering also stabilized the patterns generated by random EGMs. Overall, HDF filtering allowed an increased detection of rotors in AF patterns,

from 10.8±18.2% to 92.9±11.9% (**Figure** 7.A) and in AFL, from 10.8±18.2% to 92.9±11.9%. However, it also resulted in false detections in complex AT patterns, from 0% to 15.9±31.8% and even in random AF patterns, from 0% to 32.4±28.4%.

When solving the inverse problem of electrocardiography for AF patterns, rotors can be accurately detected even without applying HDF filtering, as it is depicted in **Figure** 6. Overall, true rotors during AF could be detected during 72.5±42.0% of time in AF patterns, with only 4.7±10.7% of time with false detections for AF, 13.2±18.0% for random EGMs and 25.0±50.0% for AFL and no false detections in the other situations (**Figure** 7.B). HDF filtering applied after inverse problem solution, increased the detection of true rotors during AF up to 80.0±44.7%, but also increased the amount of false detections in all models: i.e. 99.2±1.8% for random AF EGMs, 85.7±5.2% or random AFL EGMs or 81.9±3.1% for complex ATs.

DISCUSSION

Main findings

In this in-silico study, we have found that rotor identification based on phase singularities detection is accurate and sensitive and does not require additional signal processing in smooth signals such as unipolar EGMs, either measured or computed non-invasively. Bipolar EGMs and surface BSPM do require HDF filtering in order to detect rotors as phase singularities at the expense of a decreased specificity. HDF filtering is not recommended in the solution of the inverse problem of electrocardiography because of an increased susceptibility to detect artefactual phase singularities (see Table 1).

Phase mapping of human AF

The mechanisms of AF are still unclear because the available mapping techniques yield diverse maps ranging from organized sources to highly disordered waves[2,5,7,11,18,20]. Although phase analysis of signals has provided experimental evidence that localized re-entrant sources or rotors drive AF[7,9], it has shown conflicting results when applied to endocardial signals or body surface electrocardiographic recordings in patients. On one hand, phased-analyzed multipolar endocardial recordings showed stable and long-lasting rotors, while short-lasting rotors that tend to recur to the same anatomic location were the hallmark of inverse-computed body surface maps[5,11]. On the other hand, AF activation patterns reported using various noninvasive systems (i.e. BSMP, ECGI) using different signal processing methods appear to be simpler than epicardial maps recorded in other studies which do not report stable rotors[2,8,11]. To clarify the effect of the filtering and validate phase processing on intra-cardiac AF activity and body surface recordings, we reproduced the mapping processing in computer simulations.

Rotors and phase singularities

The phase transform has been widely used for the identification of electrical patterns in transmembrane potentials[6,19]. However, the sole detection of a phase singularity does not imply the presence of an underlying rotor, since singularities may arise from wavebreaks or fibrillatory conduction[2,9]. Nevertheless, SPs arising from wavebreaks are more unstable and do not consistently present monotonical increases in phase. In this context, other authors have already proposed to search for phase singularities in two concentric rings around the SP[18] and impose a restriction of a temporal span of at least 1 turn in order to increase specificity. In the same direction, in the present study we found that application of time and space restrictions to detected SPs allows

increasing the specificity in the detection of rotors. In particular, we propose the requirement of a good fit to a monotonical increase of phase in the 3 concentric rings. The use of 3 rings increases sensitivity as compared to a single ring, since rotors occupying a small region are detected by the inner circles while rotors with a large precession are detected by the outer rings. At the same time, the use of three rings reduces the chance for randomly distributed phases to be considered as SPs.

Phase transformation and signal morphology

We have shown that the equivalence between propagation patterns and phase maps depends on signal morphology. While the Hilbert transform results in an unambiguous phase assignment for signals with simple morphologies, for complex morphologies there is no relationship between the assigned phase values and the phase in the action potential of the tissue. Hilbert transform is mathematically defined for properly identifying the instantaneous phase value of a sinusoidal wave, assigning the whole range values from –π to π to the interval between signal peaks. However, the Hilbert transformation of complex signals with several deflections assigns the whole range of phase values from –π to π between two consecutive deflections and thus this assignment does not convey any useful information for pattern identification. We have shown that phase singularities can be detected after the phase transformation of unipolar, noise-free EGMs. However, raw EGMs with multiple deflections, such as bipolar EGMs, are not suitable for SP detection and require a pre-processing step before applying Hilbert's transform.

HDF filtering and BSPM phase mapping

We have previously proposed the use of a narrow band-pass filter prior to the

computation of the phase transformation in order to stabilize phase singularities in BSPM recordings[8]. We showed that HDF filtering allows selecting the contribution of areas that activate at the HDF while reduces the contribution on the body surface from regions that activate at a slower rate and are not harboring rotors[8]. In the present work we investigated the effect of HDF filtering on propagation patterns not maintained by rotors in order to quantify the proportion of artefactual detections introduced by our signal processing. According to our results, narrow bandpass filtering does induce false detections that can be as high as 30% in randomly distributed EGMs from AF models. For this reason, isolated SPs on BSPM maps obtained after HDF filtering, even if they last for longer than 2 turns should be interpreted with care since they are not an unequivocal demonstration of the presence of a rotational activity. However, we have shown that a high incidence of long-lasting SPs is indicative for rotational activity, since rotors were more than two-fold detected during underlying rotational patterns than for non-rotational ones.

HDF filtering of BSPM results in a particularly high incidence of detected rotational patterns in AFL models. This was to be expected because raw BSPM data already shows rotational patterns that gets stabilized by the HDF filtering. This resemblance between AF and AFL patterns can be explained by the fact that electrical potential recordings contain far-field components and, as such, the electrical sources at the vicinity of the anatomical obstacle may generate rotational electrical fields elsewhere even without an actual functional reentry source. Thus, the BSPM detection of SPs does not allow, in principle, discriminating between rotational patterns around an obstacle and functional rotors. However, here we studied the sensitivity and specificity of the BSPM to discriminate between rotational and non-rotational patterns, which is feasible and clinically relevant. Our simulations show that stable

rotational patterns on the BSPM phase maps should be considered as indicative of either AFL or AF and activation frequency should allow discriminating between these two rhythms.

HDF filtering and EGM phase mapping

A quite aggressive band-pass filtering strategy has been proposed for detecting rotational patterns in multipolar catheter baskets[5,18], similar to our HDF filtering[8]. Consistently, we have shown here that HDF filtering applied to EGMs increases the detection rate of rotors during AF at the expense of very few false detections (see Table 1). In addition, the smoothing effect of the HDF filtering appears to be necessary when the EGMs present multiple deflections so that the phase assignment by the Hilbert Transform is related to a phase in the action potential.

However, HDF filtering of EGMs results in some artefactual detections that should be taken into consideration. In particular, when the underlying pattern presents a coincidental rotation and not a mother rotor, there is an increased chance of detecting a rotor due to the smoothing effect of the HDF filtering. These coincidental rotational patterns were especially relevant in our AFL model population in which either the activation tail or anatomical obstacles give rise to non AF-driving rotations. While these coincidental rotational patterns may not fulfill the eligibility criteria for rotors because there is no single rotational center where all phases between –pi and pi converge, phase homogenization that results after HDF filtering may make these patterns as qualified for rotor detection. This effect has been also seen in both ECGI, EGM and BSPM phase maps.

HDF filtering and ECGI phase mapping

Narrow band-pass filtering has also been employed following inverse problem solution in mapping rotors during AF[9,11]. The filtering has been shown to stabilize SPs, however, we demonstrate in this study that aggressive filtering strategies applied to the inverse computed electrograms may also cause artefactual rotors. This comes as no surprise if we consider the ECGI virtual EGMs to depend on the BSPM recordings, which themselves are showing a limited sensitivity and specificity for SP and rotors detection. It is of notice though that the HDF filtering increases the detection of ECGI rotors generated by random EGMs more than for the BSPM (**Figure** 7), probably because of the additional smoothing by the inverse solution relative to the forward solution.

Limitations

The present work is based on the use of mathematical models instead of patient data because current technology does not allow determining whether detected rotors are artefactual or they are in fact AF drivers. Mathematical models, instead, allow defining specific activation patterns in which the presence of mother rotors is known a priori and thus enabled accurate classification. However, our mathematical AF models may be too simplistic and may not fully represent the whole spectra of AF patients.

Different thresholds for detection of reentrant activity had to be established, such as phase linearity or the radii of the circles for the phase assessment. The threshold election allowed increasing the specificity at the expense of decreasing the sensitivity of the reentrant activity detection, and vice versa. These thresholds were chosen to achieve a balance between specificity and sensitivity according to our database. It should be further explored whether the proposed thresholds should be

adapted to other scenarios.

Finally, we used the random distribution of the EGMs in order to generate propagation patterns with no stable reentrant patterns. Nevertheless, some of them could still retain some reentrant-like activity, due to the casual alignment of the EGMs, although in this manuscript all reentries detected in randomly patterns have been classified as false positives.

Clinical Implications

The results of the present study may have several clinical implications that should be taken into consideration during phase analysis of AF signals. First, time and space restrictions should be applied to avoid false rotors detections. To this purpose, we suggest to only consider true rotors those rotational patterns lasting >2 turns. Secondly, differentiation between AFL and AF for correct classification of rotational patterns on the BSPM phase maps should be based on activation frequency. Thirdly, selection of signals prepocessing will depend on the recording type and method. Unipolar EGMs, either recorded from the endocardium (FIRM) or those computed non-invasively (ECGI), do not require additional signal processing[5,11,16]. In contrast, endocardial bipolar EGMs and surface BSPM require HDF filtering in order to be able to detect rotors[8,18]. However, care must be taken to exclude falsely detected rotors due to the methodology. Finally, aggressive filtering strategies should be avoided during ECGI because of an increased susceptibility to stabilization and detection of false rotors (Table 1).

Conclusions

Phase transformation and singularity point identification is a robust method to identify

reentrant activity in the atrium. Smooth signals such as inverse-computed unipolar EGMs do not require additional signal processing for rotor identification. Rotor identification in signals with complex morphology such us bipolar EGMs or BSPM signals require HDF filtering to simplify the phase maps at the expense of a decreased specificity.

Funding Sources

Supported in part by: Universitat Politècnica de València through its research initiative program; Generalitat Valenciana Grants (ACIF/2013/021); the Instituto de Salud Carlos III (Ministry of Economy and Competitiveness, Spain: PI13-01882, PI13-00903, PI14/00857, PI16/01123, TEC2013-46067-R, DTS16/0160 and IJCI-2014- 22178); Spanish Society of Cardiology (Grant for Clinical Research in Cardiology 2015); Spanish Ministry of Science and Innovation Red RIC RD12.0042.0001); and the National Heart, Lung, and Blood Institute (P01-HL039707, P01-HL087226, and Q1 R01-HL118304); and cofound by FEDER.

Disclosures

FA served on the advisory board of Medtronic and Livanova. OB received research support from Medtronic and St. Jude Medical. He is a cofounder and Scientific Officer of Rhythm Solutions, Inc., Research and Development Director for S.A.S. Volta Medical and consultant to Acutus Medical. The other authors have no conflict of interest. None of the companies disclosed here financed the research described in this manuscript.

References

1. Garcia-Cosio F, Pastor-Fuentes A, Nunez-Angulo A. Clinical approach to atrial tachycardia and atrial flutter from an understanding of the mechanisms. *Rev Esp Cardiol.* 2012;65:363-75.
2. Allessie M, de Groot N. CrossTalk opposing view: Rotors have not been demonstrated to be the drivers of atrial fibrillation. *J Physiol.* 2014; 592:3167-70.
3. Narayan SM, Zaman JA. Mechanistically based mapping of human cardiac fibrillation. *J Physiol*. 2016;594:2399-415.
4. Guillem MS, Climent AM, Rodrigo M, Fernández-Avilés F, Atienza F, Berenfeld O. Presence and stability of rotors in atrial fibrillation: evidence and therapeutic implications. *Cardiovasc Res.* 2016;109:480-92.
5. Narayan SM, Krummen DE, Clopton P, Shivkumar K, Miller JM. Direct or coincidental elimination of stable rotors or focal sources may explain successful atrial fibrillation ablation: On-treatment analysis of the confirm trial. *J Am Coll Cardiol.* 2013;62:138-470.
6. Berenfeld O, Ennis S, Hwang E, Hooven B, Grzeda K, Mironov S, Yamazaki M, Kalifa J, Jalife J. Time- and frequency-domain analyses of atrial fibrillation activation rate: the optical mapping reference. *Heart Rhythm.* 2011;8:1758-65
7. Gray RA, Pertsov AM, Jalife J. Spatial and temporal organization during cardiac fibrillation. *Nature.* 1998;392:75-8.
8. Rodrigo M, Guillem MS, Climent AM, Pedron-Torrecilla J, Liberos A, Millet J, Fernandez-Aviles F, Atienza F, Berenfeld O. Body surface localization of left and right atrial high-frequency rotors in atrial fibrillation patients: A clinical-

computational study. *Heart rhythm.* 2014;11:1584-1591.

9. Vijayakumar R, Vasireddi SK, Cuculich PS, Faddis MN, Rudy Y. Methodology considerations in phase mapping of human cardiac arrhythmias. *Circ Arrhythm Electrophysiol.* 2016;9:e004409.
10. Guillem MS, Climent AM, Millet J, Arenal A, Fernández-Avilés F, Jalife J, Atienza F, Berenfeld O. Noninvasive localization of maximal frequency sites of atrial fibrillation by body surface potential mapping. *Circ Arrhythm Electrophysiol.* 2013;6:294-301.
11. Haissaguerre M, Hocini M, Denis A, Shah AJ, Komatsu Y, Yamashita S, Daly M, Amraoui S, Zellerhoff S, Picat MQ, Quotb A, Jesel L, Lim H, Ploux S, Bordachar P, Attuel G, Meillet V, Ritter P, Derval N, Sacher F, Bernus O, Cochet H, Jais P, Dubois R. Driver domains in persistent atrial fibrillation. *Circulation.* 2014;130:530-8.
12. Dössel O, Krueger MW, Weber FM, Wilhelms M, Seemann G. Computational modeling of the human atrial anatomy and electrophysiology. *Med Biol Eng Comput.* 2012;50:773-799.
13. Koivumäki JT, Seemann G, Maleckar MM, Tavi P. In silico screening of the key cellular remodeling targets in chronic atrial fibrillation. *PLoS Comput Biol.* 2014;10:e1003620.
14. García VM, Liberos A, Vidal AM, Guillem MS, Millet J, González A, Martinez-Zaldivar FJ, Climent AM. Adaptive step ODE algorithms for the 3D simulation of electric heart activity with graphics processing units. *Comput Biol Med.* 2014;44:15-26.
15. Rodrigo M, Climent AM, Liberos A, Calvo D, Fernández-Avilés F, Berenfeld O, Atienza F, Guillem MS. Identification of dominant excitation patterns and

sources of atrial fibrillation by causality analysis. *Ann Biomed Eng*. 2016;44:2364-76.

16. Pedrón-Torrecilla J, Rodrigo M, Climent AM, Liberos A, Pérez-David E, Bermejo J, Arenal Á, Millet J, Fernández-Avilés F, Berenfeld O, Atienza F, Guillem MS. Noninvasive estimation of epicardial dominant high-frequency regions during atrial fibrillation. *J Cardiovasc Electrophysiol.* 2016;27:435-42
17. Tikhonov AN. On the solution of incorrectly posed problems and the method of regularization. *Sov Math Dokl.* 1963;4:1035-1038.
18. Kuklik P, Zeemering S, van Hunnik A, Maesen B, Pison L, Lau D, Maessen J, Podziemski P, Meyer C, Schaffer B, Crijns H, Willems S, Schotten U. Identification of rotors during human atrial fibrillation using contact mapping and phase singularity detection: technical considerations. *IEEE Trans Biomed Eng.* 2016 [Epub ahead of print].
19. Zlochiver S, Yamazaki M, Kalifa J, Berenfeld O. Rotor meandering contributes to irregularity in electrograms during atrial fibrillation. *Heart rhythm.* 2008;5:846-854
20. Alhusseini M, Vidmar D, Meckler GL, Kowalewski CA, Shenasa F, Wang PJ, Narayan SM, Rappel WJ. Two independent mapping techniques identify rotational activity patterns at sites of local termination during persistent atrial fibrillation. *J Cardiovasc Electrophysiol*. 2017;doi: 10.1111/jce.13177.

Tables

		Sensitivity	Specificity
Unipolar EGMs (location criterion)	RAW	59.97%	97.94%
	HDF	68.22%	93.39%
Bipolar EGMs (location criterion)	RAW	0%	100%
	HDF	61.95%	93.35%
BSPM (presence criterion)	RAW	15.21%	100%
	HDF	89.31%	90.97%
ECGI (location criterion)	RAW	72.50%	94.27%
	HDF	80.00%	49.01%

Table 1. Sensitivity and specificity for rotor detection measurements.

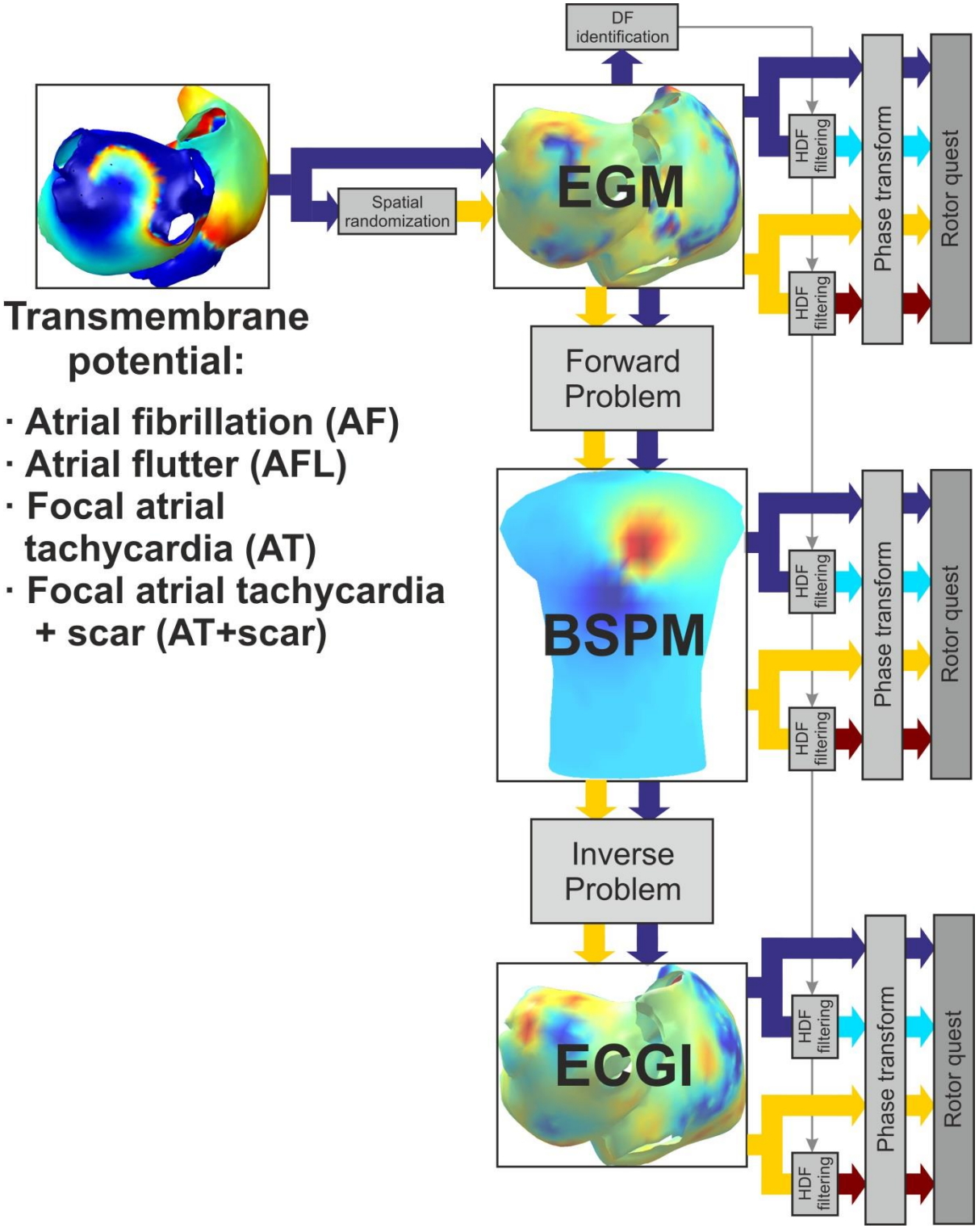

Figure 1. Workflow.

585

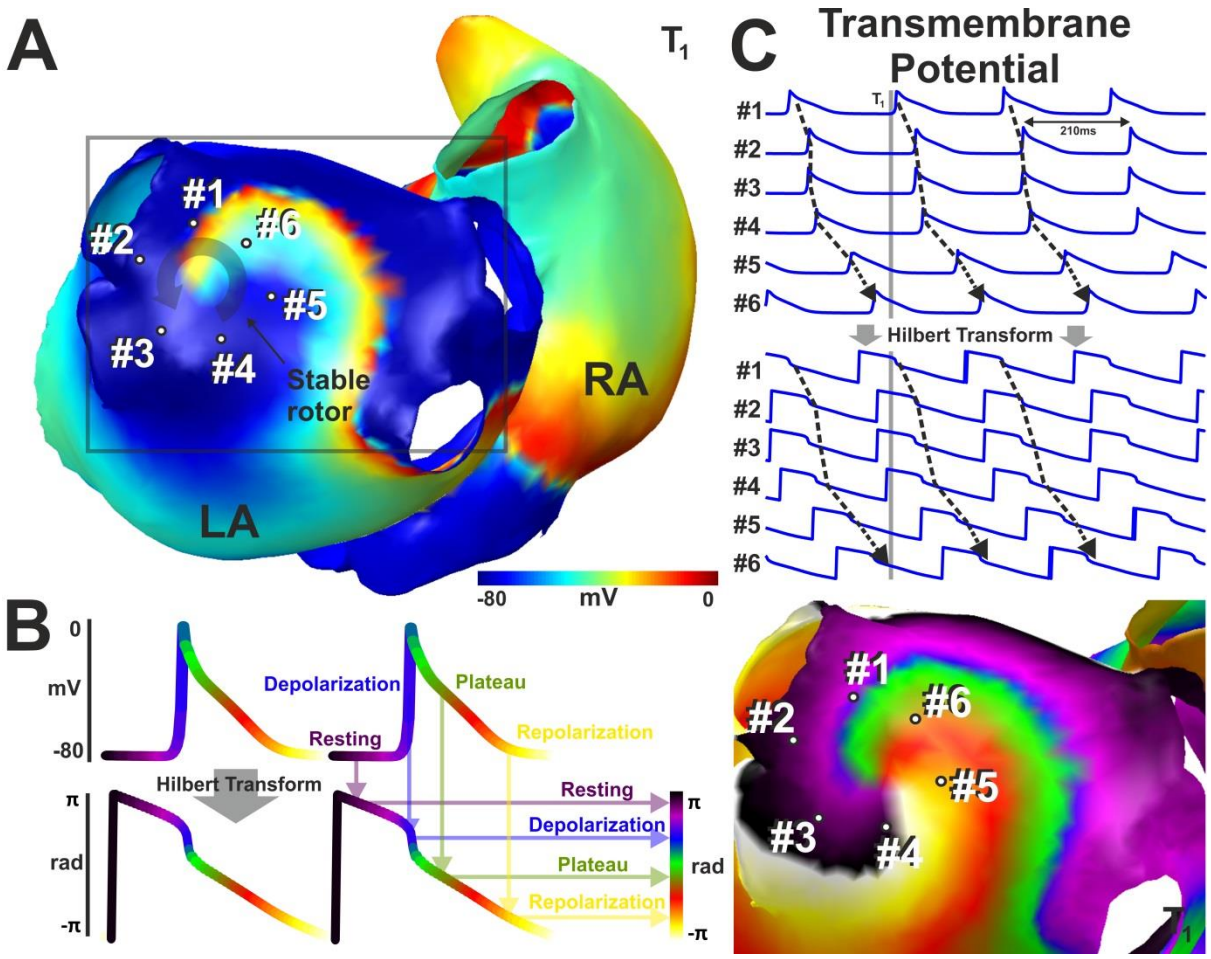

Figure 2. An example of a phase map of an atrial rotor. **(A)** Transmembrane potential map for an AF model maintained by a stable rotor in the posterior wall of the left atria. **(B)** Transmembrane potential signal (top) and its Hilbert Transform (bottom). **(C)** Transmembrane potential at 6 positions marked in (A) (top), its phase transforms (middle) and the corresponding phase map (bottom).

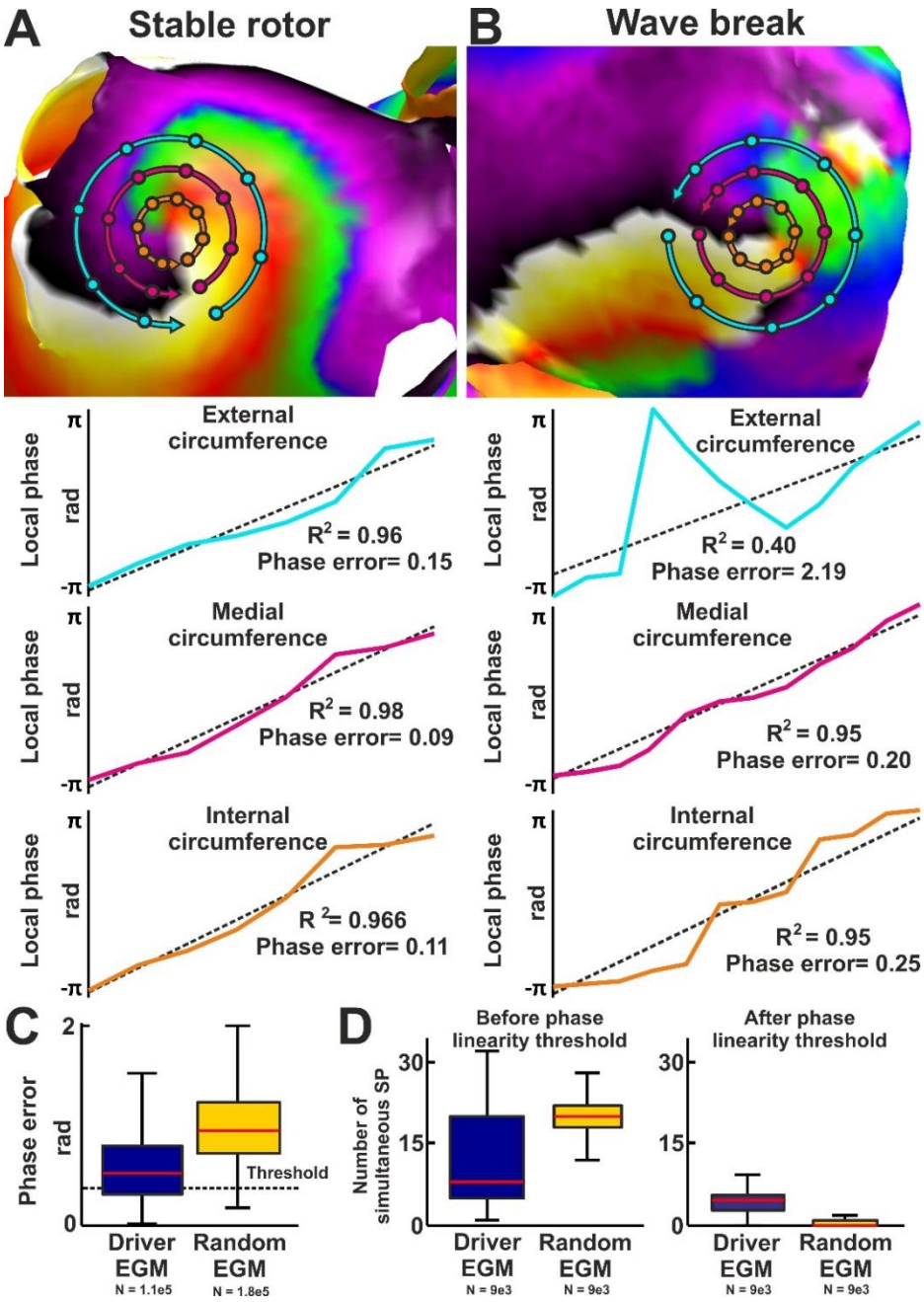

Figure 3. Phase evaluation at three concentric circles. **(A)** Phase map of transmembrane potentials from a stable rotor in the PLAW (top) and the phase values at the three concentric circles (bottom). **(B)** Phase map of transmembrane potential from a wave break (top) and the phase values at the three concentric circles (bottom). **(C)** Phase linearity error for 5 AF models. **(D)** Number or simultaneous SPs in the AF models before (left) and after (right) applying the linearity threshold.

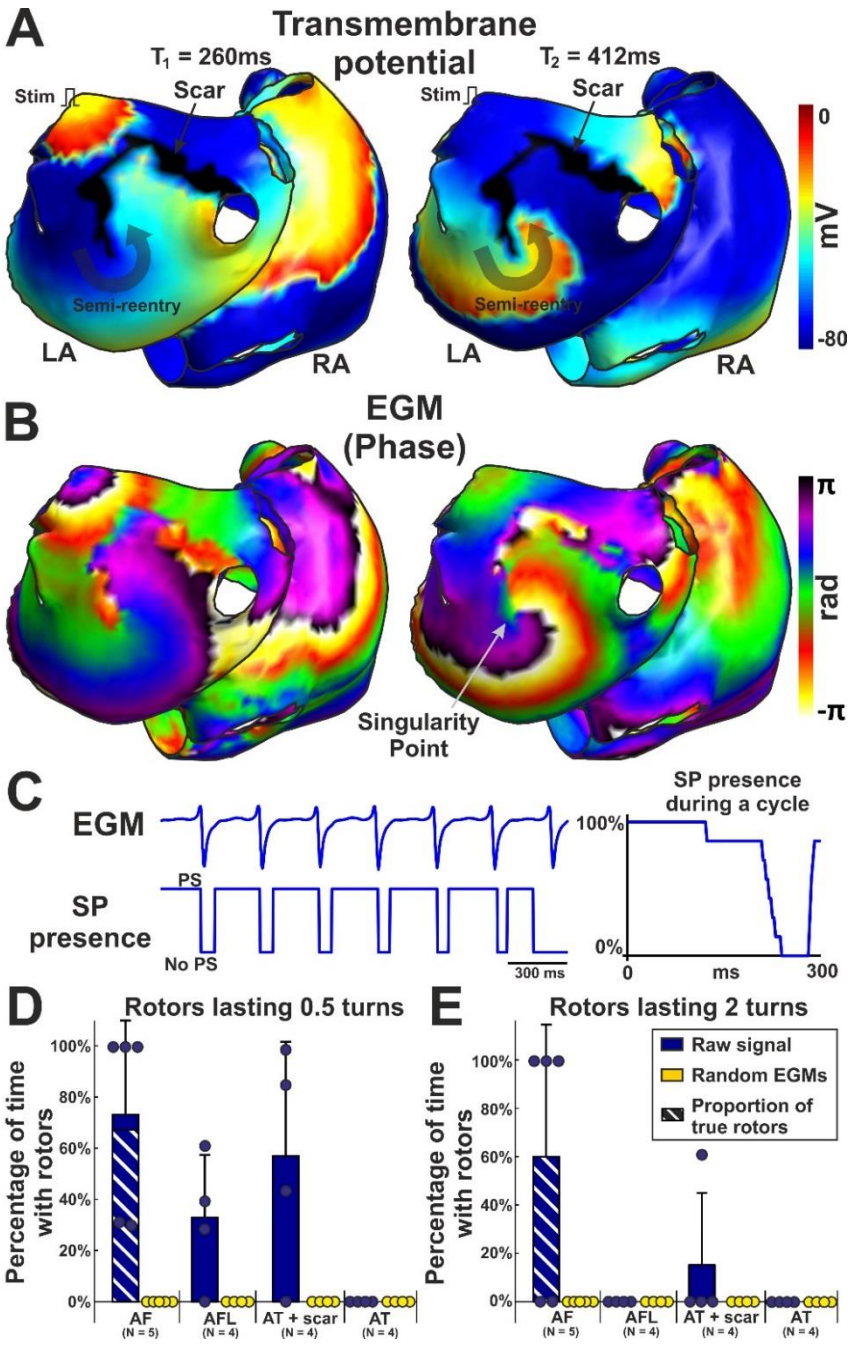

Figure 4. Temporal stability of phase singularities. **(A)** Transmembrane potential map of an AT simulation with a scar in the PLAW. **(B)** Phase map of EGM signals. **(C)** Left panel, EGM signal at the point marked with an arrow in (B); right panel, SP presence at that point has been averaged for a single cycle. **(D)** Percentage of time with rotors lasting 0.5 turns and **(E)** lasting 2 turns for the complete cohort of atrial models. Color dots represent the individual measures.

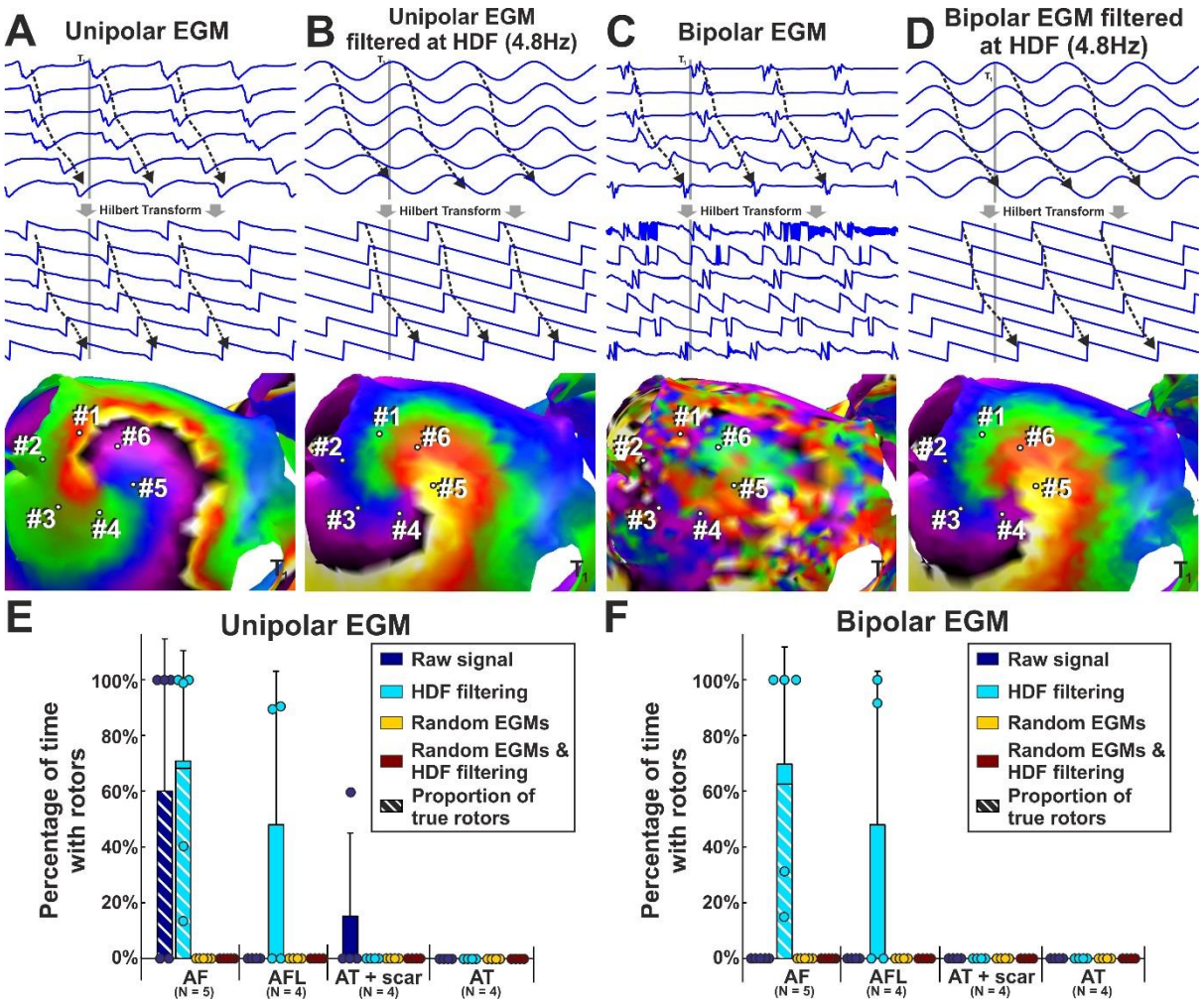

Figure 5. Phase singularity and rotor presence in EGM mapping. **(A)** Unipolar EGMs, **(B)** Unipolar EGMs filtered at the HDF, **(C)** Bipolar EGMs and **(D)** Bipolar EGMs filtered at the HDF at 6 positions (up), their phase transform (middle) and the correspondent phase map (down). **(E)** Percentage of time with rotors lasting 2 turns using unipolar signals**. (F)** Percentage of time with rotors lasting 2 turns using bipolar signals. Color dots represent the individual measures.

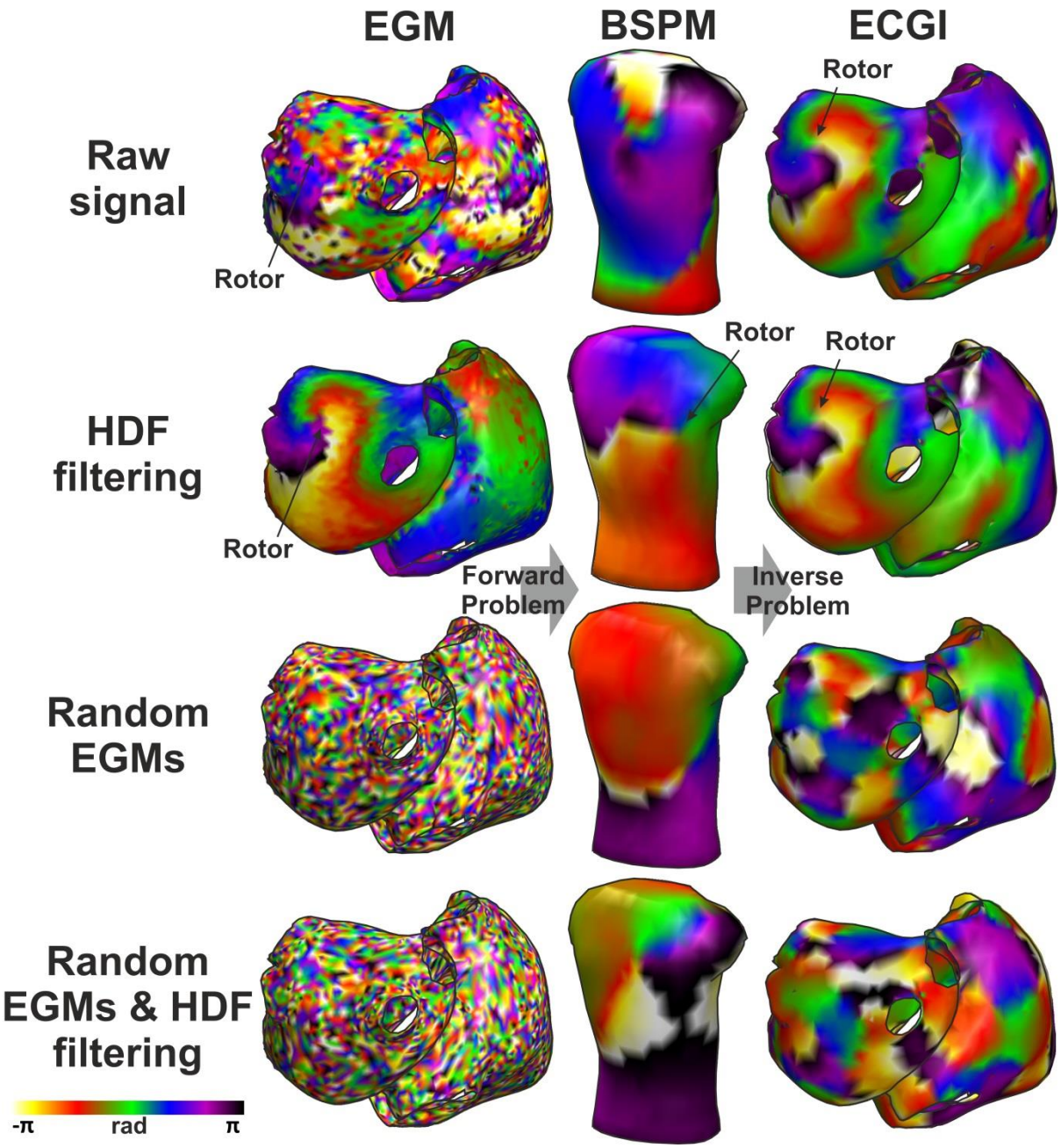

Figure 6. Example of noninvasive phase mapping and HDF filtering effect. Computed phase maps for an AF model maintained by a stable rotor in the PWLA (upper panels 1 & 2) and random EGMs (loer panels 3 & 4), together with their projection onto the torso and their backpropagation to the atrial surface (ECGi).

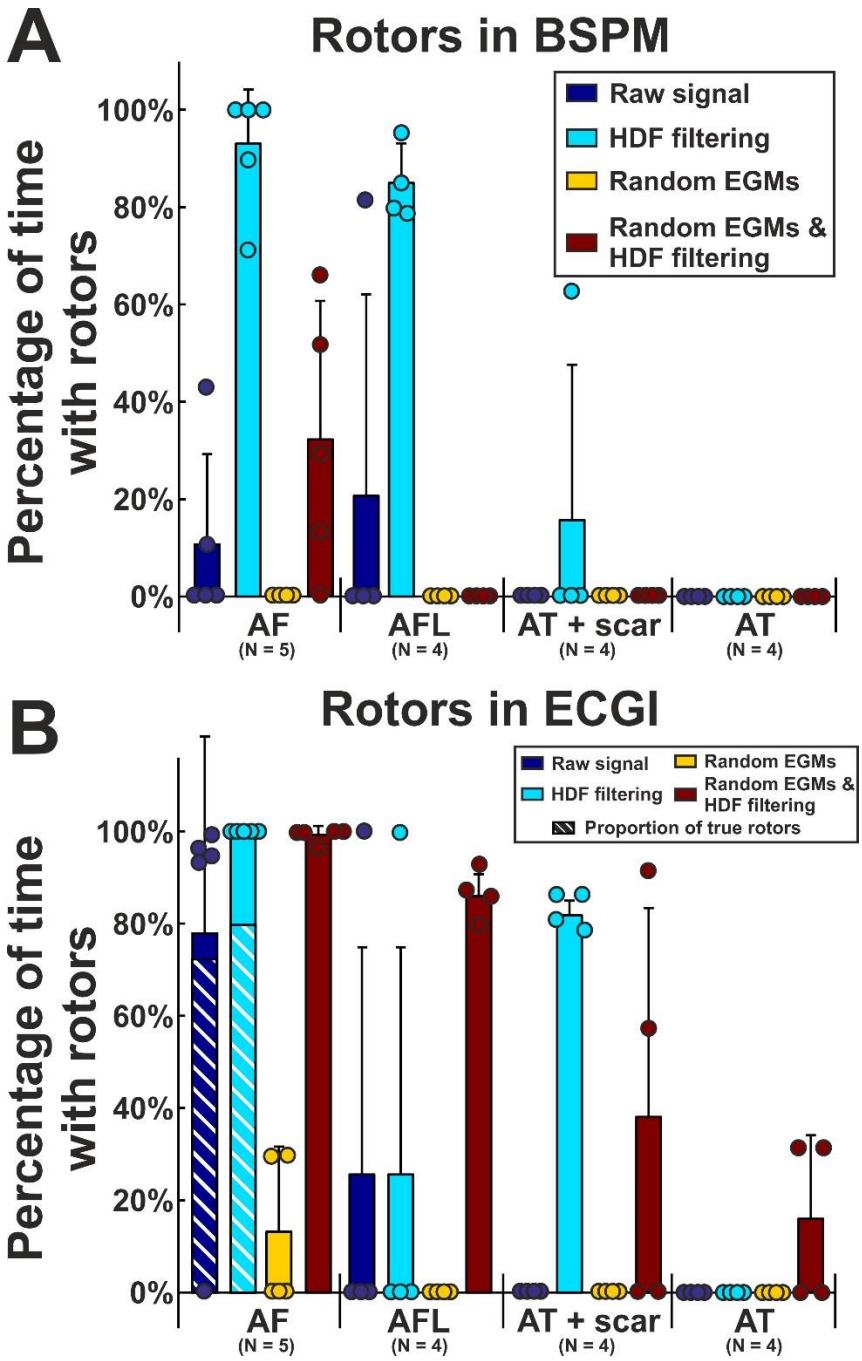

Figure 7. Rotor presence in **(A)** BSPM and **(B)** inverse-computed EGM mapping. Percentage of time with rotors lasting at least 2 turns. Color dots represent the individual measures.